CHARACTERISATION OF FOCI FORMED BY THE TELOMERIC BINDING PROTEIN POT-1 IN THE DEVELOPING *C. ELEGANS* EMBRYO

Felix H Peng

A thesis submitted to the faculty at the University of North Carolina at Chapel Hill in partial fulfilment of the requirements of the degree of Master of Science in the Curriculum of Genetics and Molecular Biology

Chapel Hill
2016

Approved by:

Shawn C Ahmed

Paul S Maddox

A Gregory Matera

ABSTRACT

Felix H Peng: Characterisation of foci formed by the telomeric binding protein POT-1 in the developing *C. elegans* embryo
(Under the direction of Shawn C. Ahmed and Paul S. Maddox)

The ends of linear chromosomes are protected by telomeres, repetitive DNA caps that are bound by a complex of proteins collectively known as shelterin. POT1, a component of shelterin, binds telomeric single stranded DNA and is important in the regulation of telomeres. Little is known about the regulation of telomeres in the context of early development. Using the early *C. elegans* embryo as a model, I have developed a system for studying telomeres in live embryos. A transgene expressing POT-1::mCherry exhibits punctate foci at telomeres during early development. Detailed analysis of this transgene in a wild-type and a telomere lengthening background suggest that telomere length may affect POT-1 binding to telomeres.

ACKNOWLEDGEMENTS

This project would not be possible without the mentorship of Shawn Ahmed and Paul Maddox. Thank you for your assistance and your patience.

I would like to thank members, past and present, of the Ahmed and MDX labs, the wide circle of colleagues and friends at SPPAR, MJC, GSC, and UNC. Thanks for all the advice, compassion, and discussion, often over wonderful food and drink. My time here would not be the same without you guys.

Finally, I would like to thank my parents for their unconditional love and support. Thanks for being my biggest cheerleaders.

TABLE OF CONTENTS

LIST OF FIGURES

LIST OF ABBREVIATIONS

ALT	alternative lengthening of telomeres
dsRNA	double-stranded RNA
h	hour(s)
kb	kilobase
mRNA	messenger RNA
µm	micrometre/micron (1×10^{-6} m)
POT-1	protection of telomeres [gene] 1
RNAi	RNA interference
ROI	region of interest
SD	standard deviation
WT	wild type

Chapter I.
INTRODUCTION

Telomeres are nucleoprotein structures that function as a cap at the ends of linear chromosomes, and are critical for genomic stability since they protect them from degradation and fusion (Blackburn 1991). Telomeric DNA is composed of tandem TTAGGG repeats in humans (Moyzis et al. 1988), with similar G-rich repeats existing in other organisms, such as TTAGGC in the nematode *Caenorhabditis elegans* (Wicky et al. 1996). Telomeric DNA contains 3′ overhangs at its most distal part (McElligott and Wellinger 1997; Raices et al. 2008); these overhangs are believed to invade itself to form a looped structure known as the T-loop (Griffith et al. 1999).

Telomeres are synthesised de novo by the reverse transcriptase telomerase (TERT), which is composed of a catalytic subunit and an RNA template (Greider and Blackburn 1989; Morin 1989). Telomerase expression is repressed in normal somatic tissue, however, it is active in germ cells and cancer cells (Kim et al. 1994). Upwards of 90% of tumour cells have activating mutations in TERT that compensate for gradual telomere shortening (Chiba et al. 2015), while the remaining proportion of tumours achieve this by a telomerase-independent pathway called alternative lengthening of telomeres (ALT) (Bryan et al. 1997).

Telomeres themselves are decorated by a complex of proteins collectively known as shelterin, which in vertebrates is composed of a core of six proteins (Figure 1A);

these are the double strand binding proteins TRF1 and TRF2, the adapter proteins RAP1, TIN2, and TPP1, and the single strand DNA binding protein POT1 (De Lange 2005). Shelterin is critical for the maintenance of telomeres, as their removal leads to telomere dysfunction and chromosome fusion caused by activation of the DNA repair machinery (Sfeir and de Lange 2012).

POT1 is found in nearly all eukaryotes and has been well studied in model organisms ranging from budding yeast to humans. It contains two, single stranded DNA binding OB fold domains at its N terminal (Lei, Podell, and Cech 2004). Stoichiometric studies of shelterin components and co-immunoprecipitation assays suggest that there is a pool of POT1 that is found away from the single-stranded telomeric DNA, presumably associating with other shelterin components interacting with double stranded DNA at the T-loop (Takai et al. 2010; Loayza and De Lange 2003). Sequence and predicted structure homology have been used to identify four homologues of POT1 in *C. elegans*. Unlike its mammalian homologues, *C. elegans* homologues of POT1 are thought to contain only one OB fold domain each; MRT-1, POT-2, and POT-3 contain an OB2 domain while POT-1 contains an OB1 domain (Raices et al. 2008; Meier et al. 2009).

C. elegans is a genetic model organism well suited for ageing studies due to its short generation time, ease of breeding, and the availability of genetic tools (Brenner 1974; Jorgensen and Mango 2002). Due to its transparent cuticle and known cell lineage, *C. elegans* is also an important model organism in studying cell biological processes and development (Sulston et al. 1983). Prior studies have established that *C.*

elegans telomeres are roughly 2 kilobases (kb) in length, and that like human telomeres, *C. elegans* telomeres form T-loops (Raices et al. 2008). For these reasons, we use this organism as a model for study of telomeres.

Prior work in our lab has shown that a POT-1::mCherry transgene localises to telomeric foci in vivo, and that both POT-1 and POT-2 repress telomerase activity (Shtessel et al. 2013). Observations from this and another independent study suggest that POT-1 and POT-2 also have a function in repressing ALT, and *pot-2* mutants were shown to have telomeres of roughly 12 kb in length after passaging for ~10 generations (Cheng et al. 2012; Shtessel et al. 2013). Our previous observations suggested that early embryos did not express POT-1 in early embryos, leading us to initially ask when telomeric foci first form during embryonic development and how they compare with telomeres in the adult germline or in larval stages of development.

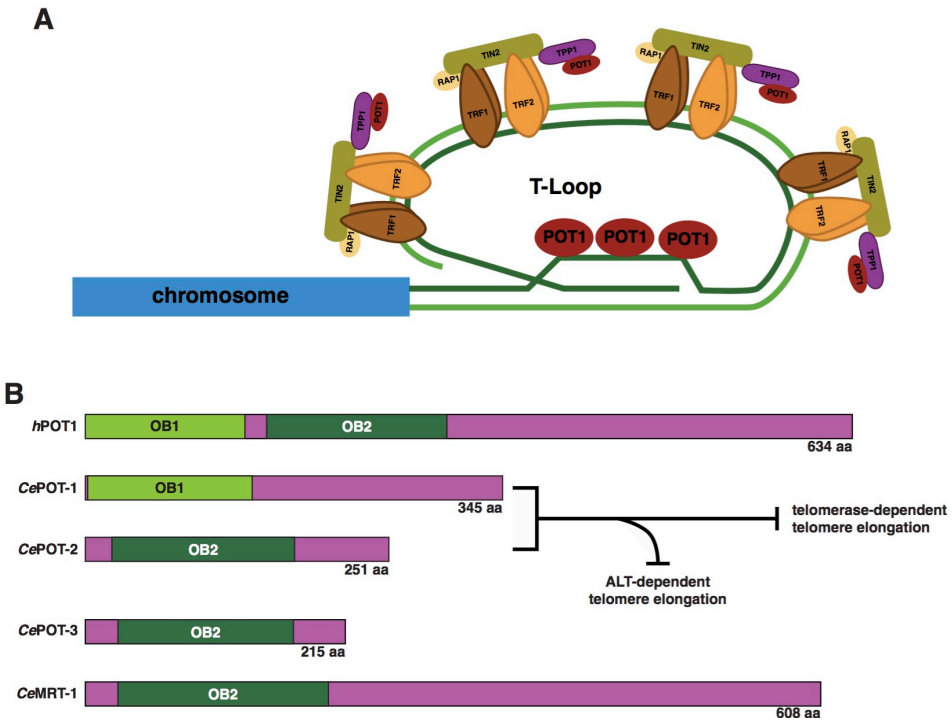

Figure 1. Schematic of the telomere and the associated shelterin complex. Telomeres form a looped structure referred to as a T-loop, which is bound by a complex of six proteins collectively known as shelterin, of which POT1 binds to single stranded DNA in a structure known as the D-loop (mammalian components and names shown in panel A). *C. elegans* homologues of human POT1. POT-1 and POT-2 have been shown to inhibit both telomerase-dependent and ALT-dependent telomere elongation (Cheng et al. 2012; Shtessel et al. 2013; B).

Chapter II.
MATERIALS AND METHODS

All strains were grown at 20°C on nematode growth medium seeded with the OP50 strain of Escherichia coli. The following strains were used during the course of this study: *pot-1::mCherry* (*yp4*), *pot-1::mCherry; pot-2*, and *dpy-7*; *unc-4*. Strains used from the Million Mutation Project (Thompson et al. 2013) are VC20684, VC40603, VC40919.

The DNA sequence of the *pot-1* 3′ UTR was synthesised as a gBlock (Integrated DNA Technologies) and directly cloned into L4440 using T4 ligase (New England Biolabs). DNA was extracted after bacterial transformation using EZNA Plasmid DNA Mini Kit (Omega Bio-Tek). After proper DNA insertion was confirmed through sequencing, the plasmid was transformed into HCT115 bacteria.

Live cell imaging of *C. elegans* embryos was performed as follows. Embryos were dissected from 7~10 gravid worms in M9 media. The embryos were then transferred to a 2% agar pad, where they were arranged in close proximity to each other with an eyelash tool. These embryos were then covered with a 1.5 thickness cover slip and sealed with Valap (**Va**seline, **La**nolin, **P**arrafin), then imaged using a DeltaVision Elite (GE Healthcare) running Softworx 5.5 (GE Healthcare). Images were acquired using a CoolSnap HQ2 CCD camera (Photometrics).

Unless otherwise noted, embryos were imaged using 60x oil immersion objective with a numerical aperture of 1.42. Z-stack images were acquired by exposure to light for .300 s per slice with a .500 µm interval between slices. Light at 32% transmission from the source was used to excite samples. To maximise POT-1::mCherry signal, images were acquired using 2x2 pixel binning.

Images were processed and analysed using Fiji (Schindelin et al. 2012). Data were input and calculated in Microsoft Excel for Mac 2011 (Microsoft Corporation). Statistical analysis and data output was performed in GraphPad Prism 6 for Windows (GraphPad Software, Inc.). Detailed protocols for image analysis is listed in the Appendix.

Chapter III.
RESULTS

Establishing a system for studying telomeric foci in live embryos. In order to understand the behaviour of telomeric foci of POT-1::mCherry, I established a system to image embryos live. Prior work performed to characterise the *pot-1::mCherry* transgene was performed in intact adult worms (Shtessel et al. 2013). However, embryos may be obscured by the highly autofluorescent gut of the animal. I thus decided to dissect out embryos for imaging. As described previously, POT-1::mCherry form bright, punctate foci in the nucleus of embryos (Shtessel et al. 2013). I attempted to image embryos using time-lapse microscopy, but found that under the conditions used, the POT-1::mCherry signal photobleached after two cell divisions, or around 15—20 minutes (Figure 2). Using this method, I observe that mCherry signal varies as cells cycle, with signal intensifying as chromosomes condense during mitosis. However, the bleaching of the signal makes it very difficult to determine the stage at which POT-1::mCherry foci persist through interphase.

I therefore elected to dissect out embryos from a number of adults and image a large population of them at a single time point. While this method prevents us from tracking an individual embryo over time, I am able to image embryos at varying stages of development. This method allows us to effectively examine the behaviour of POT-1::mCherry at different stages of development, and also maintains the variation in POT-

1::mCherry expression during early stages of embryogenesis (representative image shown in Figure 3).

POT-1::mCherry foci are visible in mitosis, but not interphase in the first cell divisions. Using this system to visualise *pot-1::mCherry* embryos, I find that POT-1::mCherry form discrete, punctate foci in the germline and in embryos, as previously reported (Shtessel et al. 2013). I observe that in earlier stages of embryogenesis (1, 2, and 4 cell stages) foci are visible in interphase at lower proportions than in later stages. However, our imaging reveals that POT-1::mCherry foci are visible during mitotic stages in these cell divisions, and that the proportion of cells with visible foci during interphase increases as embryogenesis progresses, with nearly all interphase nuclei exhibiting foci by the 8-cell stage (Figure 4A). Quantification of the number of foci in each nucleus reveals that while the number of foci per nucleus is highly variable, they appear to increase as development progresses (Figure 4B).

The number of telomeric foci differs between a telomere lengthening strain and wild-type worms. While I observe focus formation in embryos from a *pot-1::mCherry* strain, the foci are often accompanied by a nucleoplasmic haze (Figure 5A). In contrast, embryos of a *pot-1::mCherry*; *pot-2* background that had been passaged for a very long number of generations (≥F100) notably did not exhibit this diffuse expression pattern, but rather the telomeric foci were brighter and the nucleoplasmic haze was diminished (Figure 5B). I quantified the number of foci in embryos of both genotypes (Figure 5C), and found that *pot-1::mCherry*; *pot-2* embryos had a significantly higher number of foci than the otherwise wild-type (WT) strain.

Development of a quantitative measure of POT-1::mCherry focus localisation using nuclear contrast. While I clearly observed that embyros from a *pot-1::mCherry; pot-2* background had more foci and did not exhibit nucleoplasmic haze (Figure 4), I wished to be able to quantitate this otherwise qualitative observation. To that end, I established a quantitative assay based on contrast to quantify our observations. Here, I define contrast as the maximum grey value divided by the mean of the grey values within a region of interest (ROI). I reasoned that *pot-1::mCherry* embryos, with their nucleoplasmic haze, would have a lower measure of contrast than nuclei from *pot-1::mCherry; pot-2* embryos, since the maximum grey value would be divided by a much smaller number in the latter genotype (Figure 6A). Indeed, the contrast measured using this method is higher in *pot-1::mCherry; pot-2* embryos compared to those from a *pot-1::mCherry* alone background (Figure 6B).

Knockdown of endogenous POT-1 and POT-2 does not significantly alter contrast measurements compared to *pot-1::mCherry* WT worms. Since *pot-1::mCherry* strain used in these experiments contained endogenous POT-1 in addition to the mCherry tagged POT-1, I asked whether or not the depletion of endogenous POT-1 would affect the expression of POT-1::mCherry as seen in Figure 4. I reasoned that the pool of endogenous POT-1 could be competing with POT-1::mCherry for binding sites at telomeres, hypothesising that knockdown of POT-1 would lead to improved binding of POT-1::mCherry, thus increasing measured contrast. Given that *pot-2* mutations led to increased telomere length, I also asked if depletion of *pot-2* could increase contrast measurements by providing longer telomere binding sites for POT-

1::mCherry. I therefore hypothesised that POT-1::mCherry contrast measurements could be affected by depletion of *pot-2* mRNA.

C. elegans can respond bacteria expressing dsRNA to generate knockdown (Timmons and Fire 1998) and a library has been generated in *C. elegans* against nearly every known gene in its genome (Kamath et al. 2003), including *pot-1*. However, the dsRNA found here targets the entire coding region of the *pot-1* mRNA, making it inappropriate for use in our POT-1::mCherry strain. I thus generated a dsRNA that targets only endogenous *pot-1* by cloning the 3′ UTR of the gene into the L4440 vector backbone used in the Ahringer library.

pot-1::mCherry worms were picked at larval stage L4 and fed bacteria expressing two independent constructs expressing dsRNA against endogenous *pot-1* for 48h. I fed *pot-1::mCherry* worms bacteria expressing dsRNA against *pot-2* mRNA for the same amount of time. Embryos were dissected and imaged as previously described. I found that feeding dsRNA against endogenous *pot-1* and *pot-2* does not appear to alter POT-1::mCherry focus formation or contrast in a significant manner (Figure 7).

Crossing *pot-1::mCherry* with *pot-1::mCherry; pot-2* worms reveals that POT-1::mCherry foci are visible in pronuclei from *pot-2* parents. I asked if the increased contrast observed in nuclei from *pot-1::mCherry; pot-2* was parent-specific. To that end, I set up a pair of reciprocal crosses between *pot-1::mCherry* and *pot-1::mCherry; pot-2* worms. *pot-1::mCherry* hermaphrodites were mated with *pot-1::mCherry; pot-2* males, and vice versa for 24h. Embryos were dissected and time-lapse movies were made (Figure 8). As can be seen in the montages in Figure 8,

pronuclei from a *pot-1::mCherry; pot-2* background are visible before the first cell division, regardless of the parent. These results suggest that the increase in contrast that is seen in the *pot-1::mCherry; pot-2* embryos is a result of the long telomeres that are present in the *pot-2* mutant background, or perhaps a consequence of a process associated with long telomeres after growth for many generations in the absence of *pot-2*.

Worms with lengthened telomeres of varying genetic backgrounds yield an increase in foci compared to WT backgrounds. To further understand whether or not the contrast observed is due to telomeric length or by some other means, we turned to strains generated by the Million Mutation Project (Thompson et al. 2013), which generated a library of 2 007 mutagenised strains that contained mutant alleles for each of the worm's ~20 000 genes. I generated marked *pot-1::mCherry* worms to cross into three Million Mutation Project strains, all of which were shown by deep sequencing to have significantly lengthened telomeres (Thompson et al. 2013).

After crossing *pot-1::mCherry* to Million Mutation Project worms, I selected twelve F2 worms from each cross to propagate. After passaging each line for a few generations to allow for telomere lengthening, I dissected and imaged embryos as previously described. I find that the number of foci in early generations after outcrosses with the Million Mutation Project strains was often higher than for WT, but not as high as in embryos derived form very late-generation *pot-1::mCherry; pot-2* strains (Figure 9).

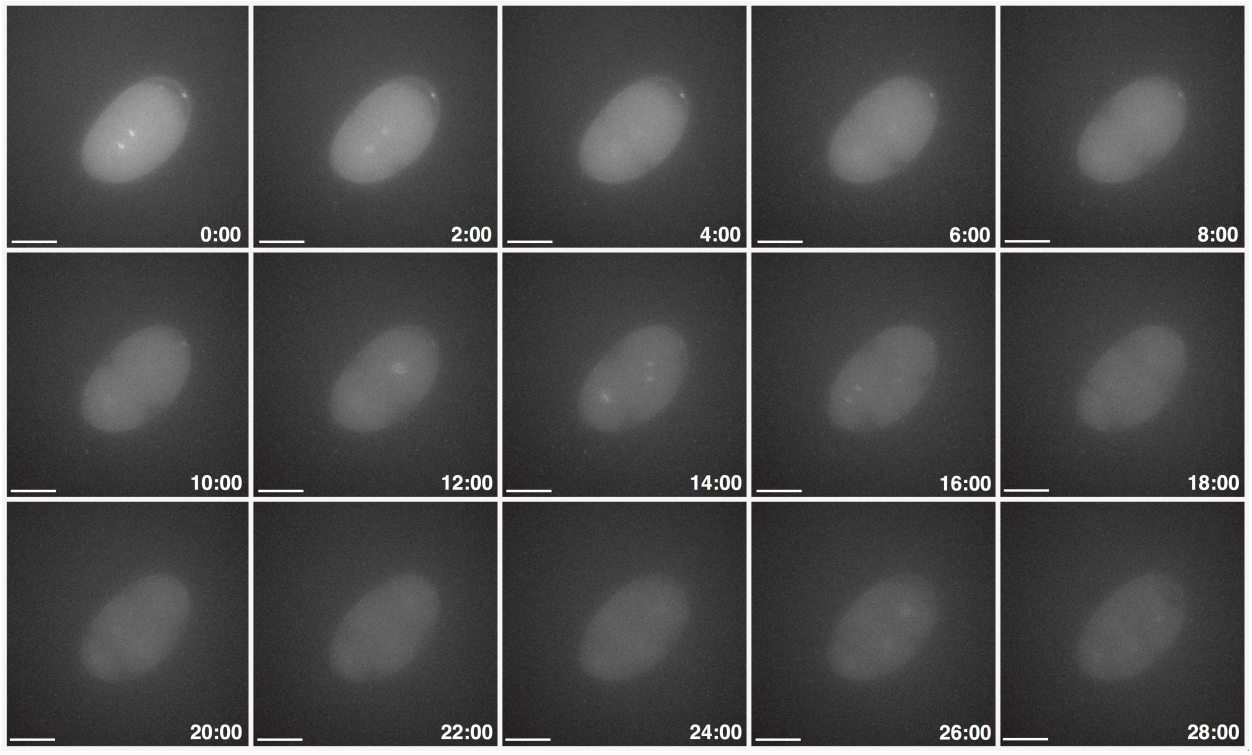

Figure 2. Montage of time-lapse images of a *pot-1::mCherry* embryo showing nearly complete photobleaching after two cell divisions. In this representative, maximum intensity montage of a *pot-1::mCherry* embryo, I see that embryos bleach after approximately two cell divisions. I observe that mCherry signal varies as cells cycle, with signal intensifying as chromosomes condense during mitosis. However, the photobleaching makes it very difficult to accurately determine the stage at which POT-1::mCherry foci persist through interphase. Scale bar represents 20 µm.

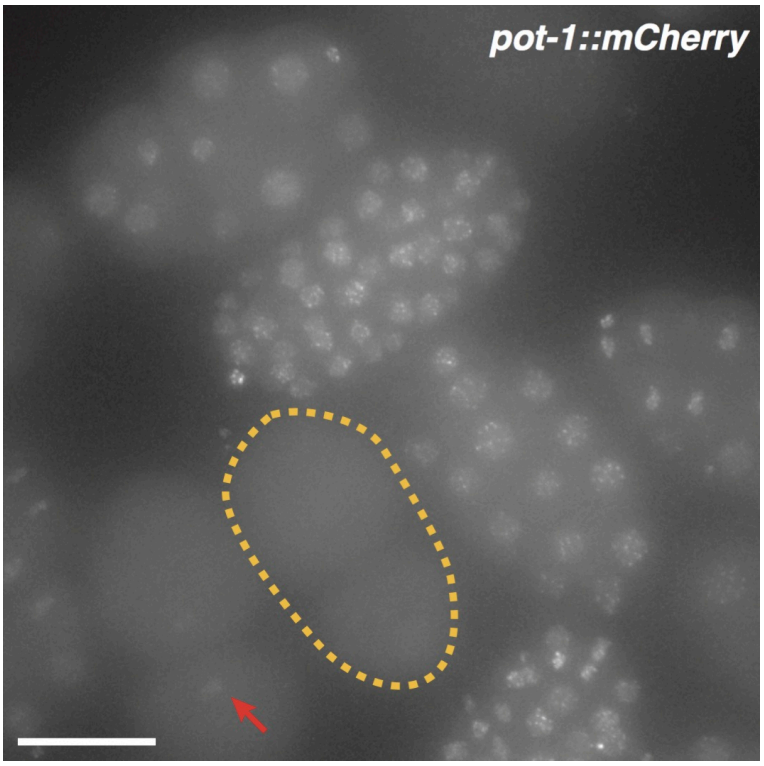

Figure 3. Embryos are imaged at single timepoints to determine the stage at which foci persist through interphase. To overcome difficulties in determining the embryonic stage at which POT-1::mCherry foci persist through interphase due to photobleaching, I dissected out embryos from 7–10 worms and imaged them at a single timepoint, thus capturing a large population of embryos at various stages of development. The dashed gold line indicates a 2-cell embryo during interphase not expressing POT-1::mCherry. The red arrowhead indicates the POT-1::mCherry signal in an embryo undergoing its first cell division. Scale bar represents 20 µm.

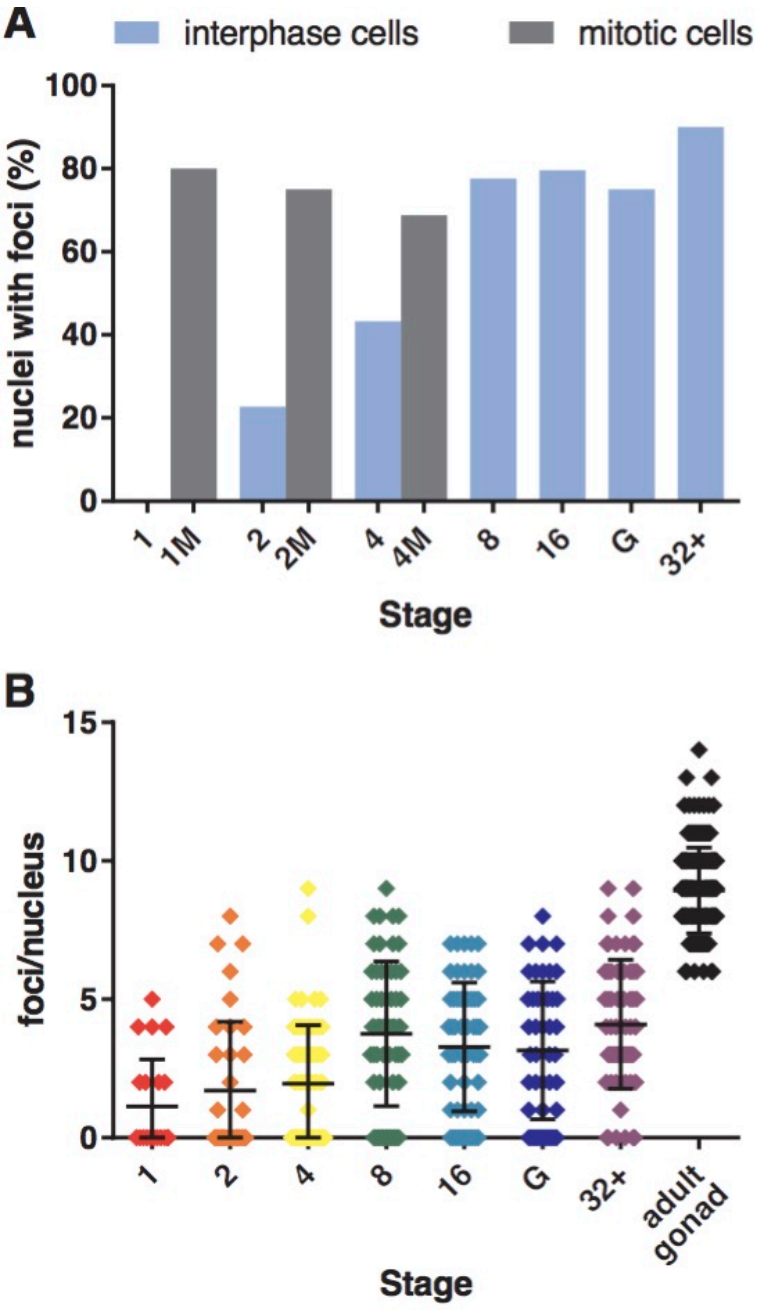

Figure 4. Quantification of embryos with persistent mCherry foci in a wild-type background. Quantification of the proportion of *pot-1::mCherry* embryos with foci during interphase (blue bars) compared to mitosis (grey) showing that while *pot-1::mCherry* embryos consistently exhibit foci during mitosis, embryos do not show persistent foci formation in interphase until the 8 cell stage (n = 335 nuclei; A). The number of foci per nucleus is highly variable, but we observe an upward trend as development progresses (B). (n = 515 nuclei analysed. Error bars in B represent SD).

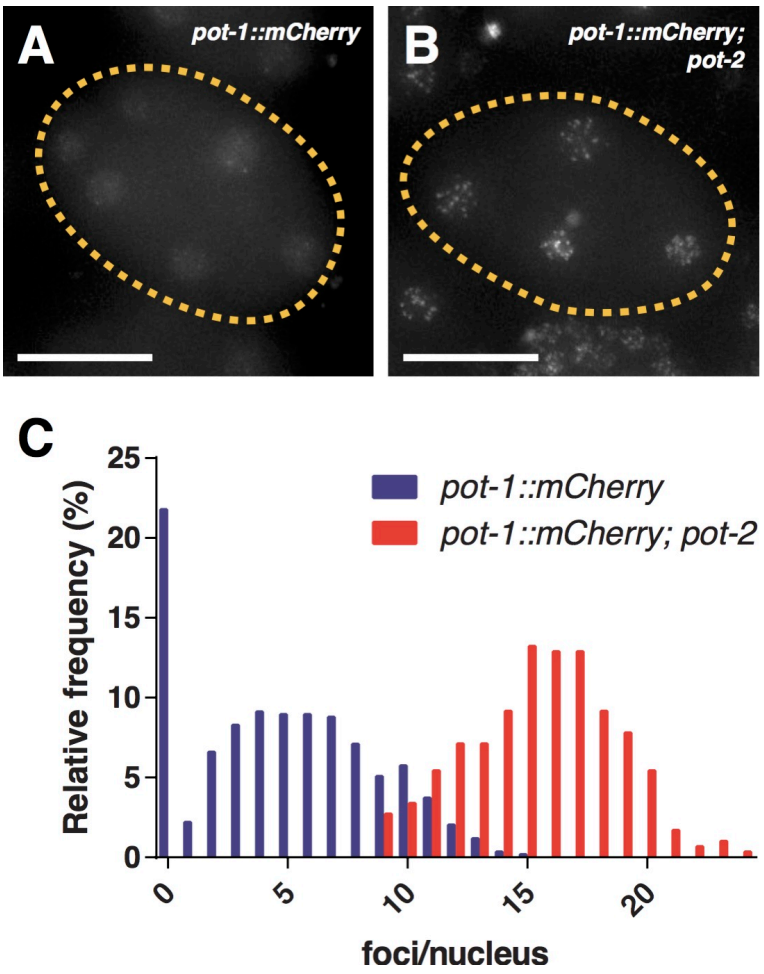

Figure 5. Localisation of POT-1::mCherry differs in different telomeric backgrounds, and the number of foci is almost doubled in a telomere lengthening background. POT-1::mCherry in an otherwise WT background shows a nucleoplasmic haze (A). POT-1::mCherry in the telomere lengthening background *pot-2* localise almost exclusively to telomeric foci (B). Histogram depicting the distribution of foci/nucleus (n = 592 *pot-1::mCherry*, 295 *pot-1::mCherry; pot-2* nuclei) Scale bars represent 20 µm.

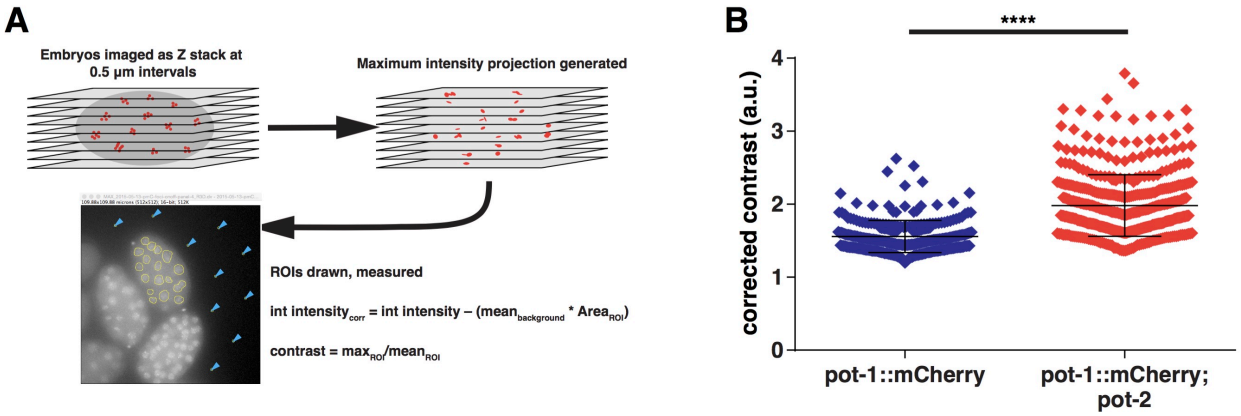

Figure 6. Development of a quantitative measure of POT-1::mCherry localisation in nuclei. Z stacks are flattened by maximum intensity projection, and ROIs are drawn around nuclei (yellow circles in panel A). Fiji is used to calculate the maximum grey value and the mean grey value within the ROI, and contrast is calculated by dividing the former by the latter. I find that *pot-1::mCherry; pot-2* worms have significantly higher contrast measurements than their WT counterparts, with an increase in mean contrast of 27.1% (n = 269 WT, 431 *pot-1::mCherry; pot-2* nuclei, B).

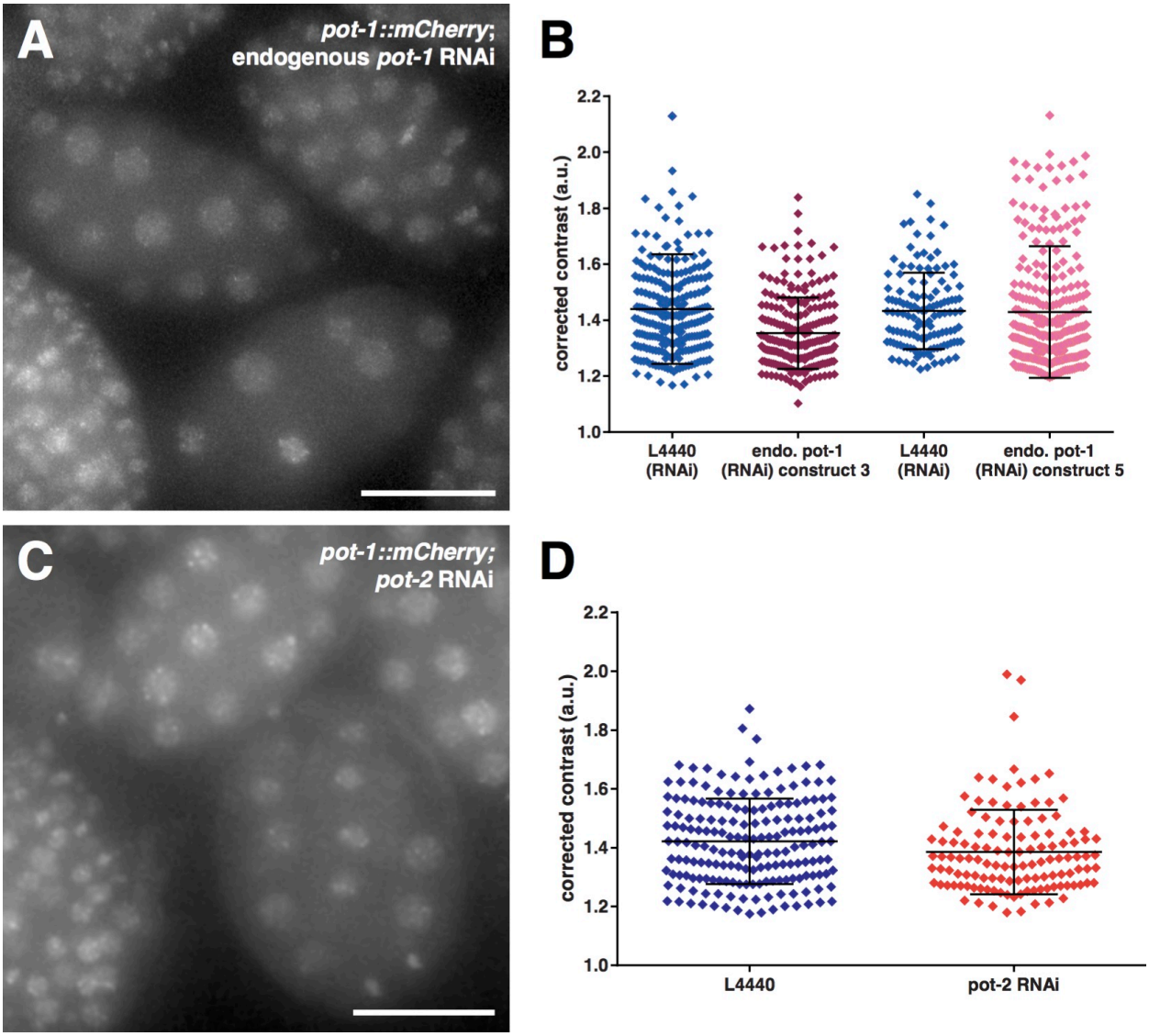

Figure 7. Knockdown of endogenous *pot-1* and *pot-2* does not appear to noticeably affect contrast or focus formation. Representative images of embryos fed dsRNA against endogenous *pot-1* (A) and *pot-2* (C). Contrast measurements for two independent plasmids against endogenous *pot-1* yield no significant increase in contrast after 48h feeding (n = 222 nuclei *endo pot-1 construct 3*, 247 nuclei *construct 3 L4440* (ctrl); n = 247 nuclei *endo. pot-1 construct 5*, 318 nuclei *construct 5 L4440* (ctrl); B). 48h RNAi feeding against *pot-2* does not result in a significant increase in nuclear contrast (n = 185 nuclei *L4440*, 123 nuclei *pot-2 RNAi*; D). Scale bars represent 20 µm. Error bars represent SD.

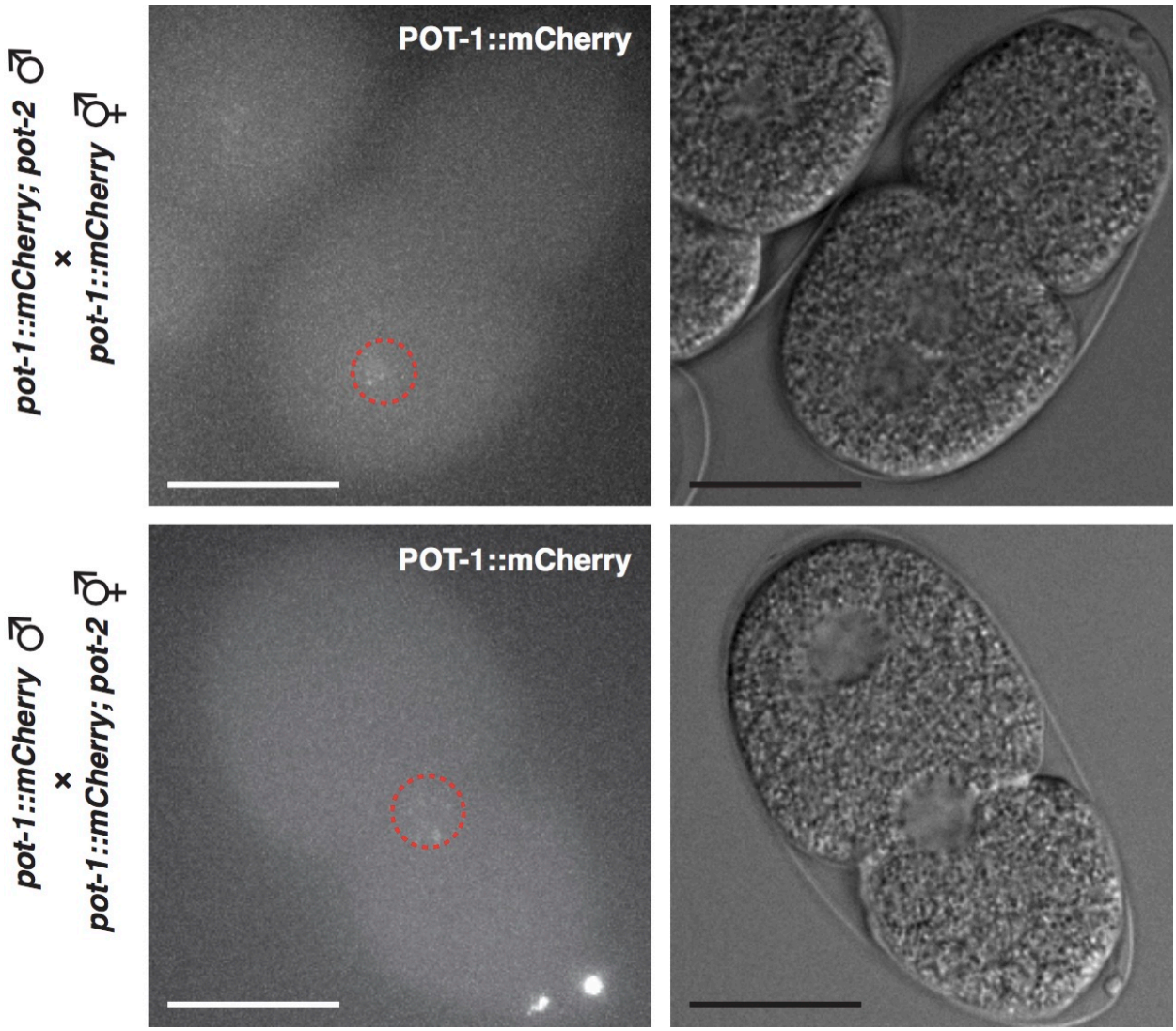

Figure 8. POT-1::mCherry foci are visible in pronuclei derived from ALT-dependent telomere lengthening mutants. *pot-1::mCherry; pot-2* males were crossed with *pot-1::mCherry* hermaphrodites (top row, DIC reference image on right), as was a reciprocal cross (bottom row, DIC reference image on right). Even before pronuclear fusion, POT-1::mCherry foci are visible in the pronucleus derived from the *pot-2* background with elongated telomeres. Scale bars represent 20 µm.

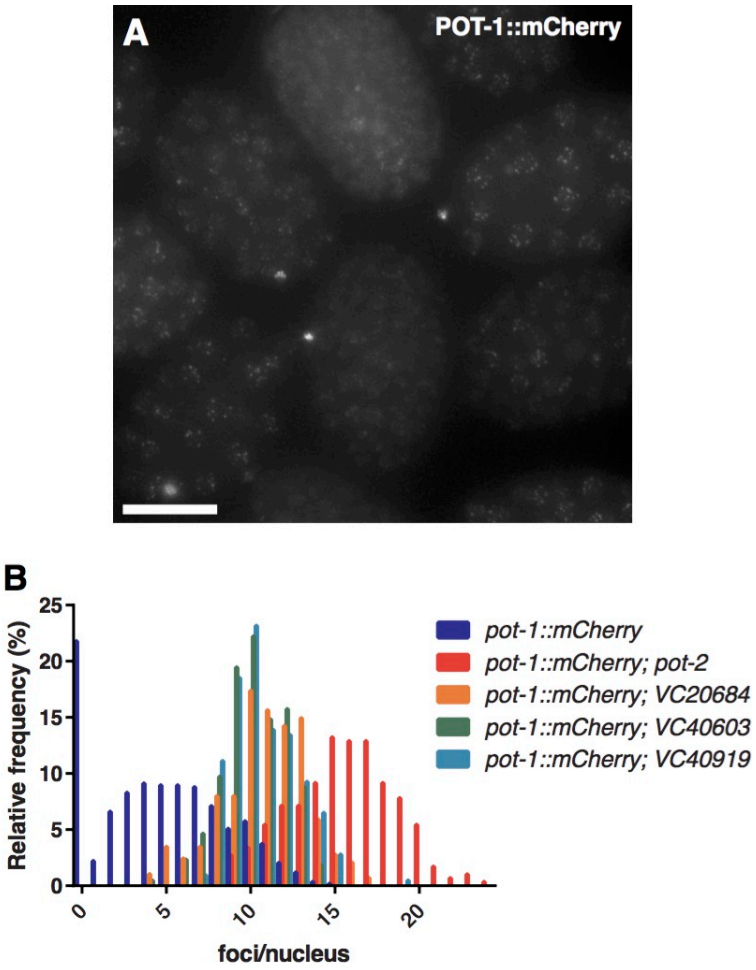

Figure 9. Million Mutation Project strains with lengthened telomeres exhibit an increase in the number of foci counted per nucleus. Representative maximum intensity projection of *pot-1::mCherry* crossed to Million Mutation Project strains with lengthened telomeres (A). Quantitation of foci of these worms reveal an increase in the number of foci per nucleus in long telomere strains versus *pot-1::mCherry* alone, though the number of foci is not as high as seen in the ALT mutant *pot-2* background (n = 592 *pot-1::mCherry*, 295 *pot-1::mCherry; pot-2*, 288 *pot-1::mCherry; VC20684*, 216 *pot-1::mCherry; VC40603*, 216 *pot-1::mCherry; VC40919* nuclei B). Scale bars represent 20 μm.

Chapter IV.
DISCUSSION

Here I have performed detailed analysis of the telomere binding protein POT-1 during early development. By employing live-cell imaging, we have determined that POT-1::mCherry foci appear persistently through the cell cycle at around the 8-cell stage, with POT-1::mCherry signal appearing only during mitosis in stages before then. I have also determined that the number of foci per nucleus increases as development progresses (Figure 4). Using nuclear contrast as a quantitative measure of POT-1 binding to foci, I observe that telomeric localisation of POT-1::mCherry increases in backgrounds of increased telomere length. Specifically, I examined POT-1::mCherry localisation in strains that either contained a known ALT phenotype (*pot-2*) or with several mutations that can cause long telomeres (Million Mutation Project).

In this study, I compare the expression of POT-1::mCherry in a WT and *pot-2* background in which telomeres have had many generations to increase in length. I observed that POT-1::mCherry expresses in a diffuse nucleoplasmic pattern in WT worms (Figure 5A), but that this diffuse expression is absent in a background where telomeres have been elongated via ALT (Figure 5B). Our data therefore suggest that in the telomere lengthening background, POT-1::mCherry localises to a greater number of more intense foci.

I asked if the abundance of endogenous, untagged POT-1 protein could be affecting the localisation of our tagged transgene. By using RNAi against endogenous POT-1, I could not measure a significant difference in contrast (Figure 7). Similarly, when asking if an acute (48h) knockdown of *pot-2* could trigger ALT-dependent telomere lengthening, I was unable to measure a significant difference in contrast. In fact, mean contrast appears to have decreased in *pot-2* knockdown worms compared to a feeding control. While my results suggest that there is not a significant difference in contrast between the POT-1::mCherry signal fed a control vector and the knockdowns we generated, we cannot rule out that the RNAi may not have been effective. Since no antibody against POT-1 or POT-2 has been reported to our knowledge, we are unable to probe the effectiveness of RNAi knockdown by western blotting. Validation of knockdowns of both genes tested will be important controls to conduct in future experiments. Additional experiments using genetic nulls of both endogenous *pot-1* and *pot-2* may also be effective in helping us understand these questions.

I was unable to answer whether or not length could be a factor affecting POT-1::mCherry association with telomeres through RNAi. However, genetic evidence suggests that telomere length may indeed affect POT-1::mCherry binding to telomeres. Importantly, I generated males of both *pot-1::mCherry* and *pot-1::mCherry; pot-2*. These males were crossed to hermaphrodites of the opposing genotype, and time-lapse imaging was used to track the pronuclei of both parents as fertilisation occurred. Our resulting movies revealed that only the pronucleus derived from the parent with a *pot-2* mutant background had any visible foci, and that these foci were visible throughout the

process of pronuclear fusion (Figure 9). Given that the *pot-2* mutants were passaged for many (≥100) generations and presumably have very long telomeres, these data suggest either that telomere length could be a significant factor in determining the amount of POT-1 binding, or that the absence of POT-2 in pronuclei lead to the presence of POT-1 foci in 1 cell stage nuclei prior to mitosis.

The worm strains used in this study contain a *pot-1::mCherry* transgene generated by the mosSCI single copy insertion protocol (Frokjaer-Jensen et al. 2014) to allow for the targeted insertion of a transgene at a defined location in the genome. While the *pot-1::mCherry* strain used in this study is a valuable tool for studying telomeres in vivo, there are shortcomings. Notably, *pot-1::mCherry* is not expressed under the endogenous *pot-1* promoter, instead being expressed under the germline specific *daz-1* promoter (Maruyama et al. 2005). The POT-1::mCherry signal I observed could be a result of POT-1 overexpression, as endogenous *pot-1* was not ablated. To address this, it is possible that Cas-9 mediated genome editing may be employed to tag endogenous *pot-1* with either GFP or mNeonGreen (Cong et al. 2013; Mali et al. 2013; Dickinson et al. 2013; Dickinson et al. 2015). However, these efforts have not been successful to date (Table 1 summarises the primers used in these efforts).

Our data suggest a model by which long telomeres correlate with greater binding of POT-1::mCherry, accounting for the increased number of foci and increased intensities of foci observed in the *pot-2* mutant background (Figure 10). We can speculate that prolonged loss of *pot-2* or an epigenetic state that accompanies long telomeres in combination with *pot-2* deficiency could also lead to these phenotypes.

POT-1 binds single stranded DNA at telomeres specifically (Lei, Podell, and Cech 2004), but it is thought that a fraction of POT-1 is also found at other parts of the telomere (De Lange 2005; Palm and de Lange 2008; Takai et al. 2010), most likely in association with other shelterin components. In the *pot-2* deletion background, telomeres have elongated significantly after many generations of passaging, thus providing a longer binding substrate for shelterin components, and especially POT-1, to associate with. This could imply increased single stranded DNA at elongated telomeres. Given that POT-1 foci in early embryos can be observed in parental pronuclei derived from *pot-1::mCherry; pot-2* gametes, my observations suggest that telomere length, possibly in combination with loss of POT-2*,* could contribute to visibility of POT-1 foci in early embryos. One could speculate that the presence of these foci could reflect increased telomerase activity or increased activity of the telomerase independent telomere elongation pathway ALT. Future work may address these possibilities.

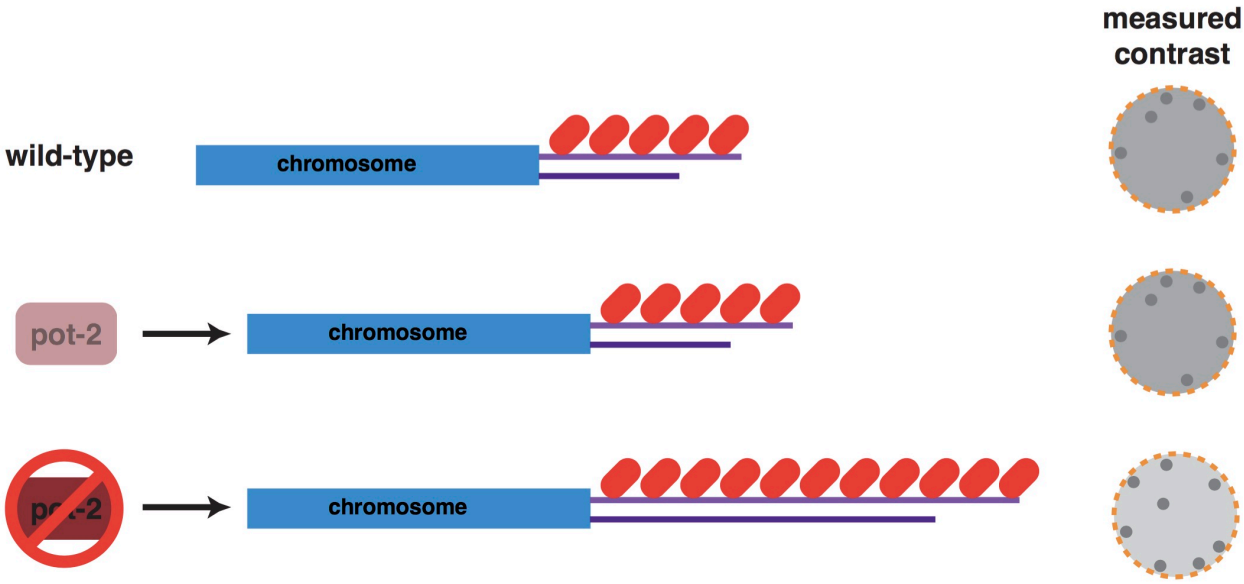

Figure 10. Model for telomeric focus formation in a wild-type versus telomere-lengthening background. WT telomeres are roughly 2 kb in length (Raices et al. 2008), yielding baseline contrast measurements. Knockdown of *pot-2* does not appear to appreciably alter contrast, but a genetic mutant of the gene appears that has been passaged for many generations does. This is suggestive of a model in which the loss of POT-2, the lengthening of telomeres, or both, may perturb the localisation of POT-1::mCherry to telomeres.

Table 1. List of primers used in attempts to endogenously tag POT-1 using CRISPR. List of primers used in attempts to endogenously tag POT-1 using the SEC protocol developed by Dickinson and colleagues (Dickinson et al. 2015). All primers are listed in 5′ to 3′ direction.

Name	Sequence
pot1-5-fwd	ACGTTGTAAAACGACGGCCAGTCGCCGGCATGTCGGTTCTGTCAAG GTTAGCC
pot1-5-rev	CATCGATGCTCCTGAGGCTCCCGATGCTCCAATATTAATATTGTAGAA AACAACTTCGG
pot1-3-fwd	CGTGATTACAAGGATGACGATGACAAGAGAGATATTCATCTCTCCGA AGTTGTTTTCTAC
pot1-3-rev	GGAAACAGCTATGACCATGTTATCGATTTCAGAAATCTCTGGGCCAC CAACAG
p1-SDMF	GAAGTTGTTTTCTACAATATTAATATTGGAGCATC
p1-SDMR	GGAGAGATGAACAATTGACTTCAATTCAAGTGAAC

APPENDIX: Image Analysis Protocols

Part I. Measurement of contrast is performed according to the following protocol:

1. Image is opened in Fiji. If image was acquired as a panel image, a Bio-Formats Series Options window will open, prompting the user to select the panels of interest.

2. Brightness and contrast are reset, either manually (in single panels using Brightness and Contrast tool) or by “Reset Min Max” macro (batch processing, source code can be found at the end of this section).

3. For contrast measurements, panels are Z projected manually (individual panels, or panels requiring a projection of a subset of total slices) or via “Batch MIP” macro (source code can be found at the end of this selection).

4. ROIs are selected using freehand selection tool with the aide of a Wacom Intuos tablet and added to Fiji’s integrated ROI manager.

5. For background noise correction, 10 circular ROIs 7 pixels in diameter are selected in the background (i.e. non-cytoplasmic, non-embryonic signals), and included as the final ROIs in the ROI manager.

6. ROIs in ROI manager are measured, with the following parameters being recorded (measurements can be set using “Analyze > Set Measurements…” command in the Fiji Menu Bar):

Area – Area of ROI

Mean – Average grey value of ROI

StdDev – Standard deviation of grey values of ROI

Min – Minimum grey value in ROI

Max – Maximum grey value in ROI

IntDen – Integrated density, this is the product of the area and mean grey value. **It is important to note that this value should not be used in our calculations. Inclusion of this value is necessary to obtain measurements of RawIntDen.**

RawIntDen – Raw integrated density, also known as Integrated Intensity, is the sum of the all pixel values in the ROI being measured. It is not to be confused with the Integrated Density measurement used in Fiji. **We use this measurement in our calculations.**

7. Measured values in Results window are copied to an Excel worksheet.

8. Average background is calculated by averaging the mean values of the background ROIs selected in step 5.

9. Corrected Mean and Max are calculated by subtracting value calculated in step 8 from measured mean and max values.

10. Corrected contrast is calculated by dividing corrected maximum value by corrected mean value.

Part II. Measurement of Integrated Intensity is performed identically to steps 1–8 in Part I. The calculated average background is multiplied by the area of the ROI. This value is then subtracted from the Integrated Intensity value obtained in step 6 of Part I.

Part III. Focus counts are performed manually. The image panel is opened as in steps 1 and 2 in Part I. Nuclear foci are counted in each slice, and are marked using the

Multi-point tool in Fiji. The number of points are counted, and the resulting value input into Excel.

Part IV. Source code for “Reset Min Max”

```
for (id = 1; id <= nImages(); id++)
{
    selectImage(id);
    resetMinAndMax();
}
```

Part V. Source code for “Batch MIP”

```
for (id = 1; id <= nImages(); id++)
{
    selectImage(id);
    resetMinAndMax();
    run("Z Project...", "projection=[Max Intensity]");
}
```

REFERENCES

Blackburn, E H. 1991. “Structure and Function of Telomeres.” *Nature* 350 (6319): 569–73. doi:10.1038/350569a0.

Brenner, S. 1974. “The Genetics of Caenorhabditis Elegans.” *Genetics* 77 (1): 71–94. doi:10.1002/cbic.200300625.

Bryan, T M, A Englezou, L Dalla-Pozza, M A Dunham, and R R Reddel. 1997. “Evidence for an Alternative Mechanism for Maintaining Telomere Length in Human Tumors and Tumor-Derived Cell Lines.” *Nature Medicine* 3 (11): 1271–74. doi:10.1038/nm1197-1271.

Cheng, Chen, Ludmila Shtessel, Megan M Brady, and Shawn Ahmed. 2012. “Caenorhabditis Elegans POT-2 Telomere Protein Represses a Mode of Alternative Lengthening of Telomeres with Normal Telomere Lengths.” *Proceedings of the National Academy of Sciences of the United States of America* 109 (20): 7805–10. doi:10.1073/pnas.1119191109.

Chiba, Kunitoshi, Joshua Z. Johnson, Jacob M. Vogan, Tina Wagner, John M. Boyle, and Dirk Hockemeyer. 2015. “Cancer-Associated Tert Promoter Mutations Abrogate Telomerase Silencing.” *eLife* 4 (JULY 2015): 1–20. doi:10.7554/eLife.07918.

Cong, Le, F. Ann Ran, David Cox, Shuailiang Lin, Robert Barretto, Naomi Habib, Patrick D. Hsu, et al. 2013. “Multiplex Genome Engineering Using CRISPR/Cas System.” *Science* 339 (February): 819–24. doi:10.1126/science.1231143 RNA-Guided.

De Lange, Titia. 2005. “Shelterin: The Protein Complex That Shapes and Safeguards Human Telomeres.” *Genes and Development* 19 (18): 2100–2110. doi:10.1101/gad.1346005.

Dickinson, Daniel J, Jordan D Ward, David J Reiner, and Bob Goldstein. 2013. “Engineering the Caenorhabditis Elegans Genome Using Cas9-Triggered Homologous Recombination.” *Nature Methods* 10 (10): 1028–34. doi:10.1038/nmeth.2641.

Dickinson, Daniel J., Ariel M. Pani, Jennifer K. Heppert, Christopher D. Higgins, and Bob Goldstein. 2015. “Streamlined Genome Engineering with a Self-Excising Drug Selection Cassette.” *Genetics* 200 (4): 1035–49. doi:10.1534/genetics.115.178335.

Frokjaer-Jensen, Christian, M Wayne Davis, Mihail Sarov, Jon Taylor, Stephane Flibotte, Matthew LaBella, Andrei Pozniakovski, Donald G Moerman, and Erik M Jorgensen. 2014. “Random and Targeted Transgene Insertion in C. Elegans Using a Modified Mosl Transposon.” *Nat. Methods* 11 (5): 529–34.

doi:10.1038/nmeth.2889.Random.

Greider, Carol W., and Elizabeth H. Blackburn. 1989. “A Telomeric Sequence in the RNA of Tetrahymena Telomerase Required for Telomere Repeat Synthesis.” *Nature* 337: 331–37.

Griffith, Jack D., Laurey Comeau, Soraya Rosenfield, Rachel M. Stansel, Alessandro Bianchi, Heidi Moss, and Titia De Lange. 1999. “Mammalian Telomeres End in a Large Duplex Loop.” *Cell* 97 (4): 503–14. doi:10.1016/S0092-8674(00)80760-6.

Jorgensen, Erik M, and Susan E Mango. 2002. “The Art and Design of Genetic Screens: Caenorhabditis Elegans.” *Nature Reviews. Genetics* 3 (5): 356–69. doi:10.1038/nrg794.

Kamath, Ravi S, Andrew G Fraser, Yan Dong, Gino Poulin, Richard Durbin, Monica Gotta, Alexander Kanapin, et al. 2003. “Systematic Functional Analysis of the Caenorhabditis Elegans Genome Using RNAi.” *Nature* 421 (6920): 231–37. doi:10.1038/nature01278.

Kim, Nam W, Mieczyslaw a Piatyszek, Karen R Prowse, Calvin B Harley, D West, Peter L C Ho, Gina M Coviello, et al. 1994. “Specific Association of Human Telomerase Activity with Immortal Cells and Cancer.” *Science* 266 (December 1994): 2011–15. doi:10.1126/science.7605428.

Lei, Ming, Elaine R Podell, and T R Cech. 2004. “Structure of Human POT1 Bound to Telomeric Single-Stranded DNA Provides a Model for Chromosome End-Protection.” *Nature Structural & Molecular Biology* 11 (12): 1223–29. doi:10.1038/nsmb867.

Loayza, Diego, and Titia De Lange. 2003. “POT1 as a Terminal Transducer of TRF1 Telomere Length Control.” *Nature* 423 (6943): 1013–18. doi:10.1038/nature01688.

Mali, Prashant, Luhan Yang, Kevin M Esvelt, John Aach, Marc Guell, James E DiCarlo, Julie E Norville, and George M Church. 2013. “RNA-Guided Human Genome Engineering via Cas9.” *Science (New York, N.Y.)* 339 (6121): 823–26. doi:10.1126/science.1232033.

Maruyama, Rika, Sachiko Endo, Asako Sugimoto, and Masayuki Yamamoto. 2005. “Caenorhabditis Elegans DAZ-1 Is Expressed in Proliferating Germ Cells and Directs Proper Nuclear Organization and Cytoplasmic Core Formation during Oogenesis.” *Developmental Biology* 277 (1): 142–54. doi:10.1016/j.ydbio.2004.08.053.

McElligott, Richard, and Raymund J. Wellinger. 1997. “The Terminal DNA Structure of Mammalian Chromosomes.” *EMBO Journal* 16 (12): 3705–14. doi:10.1093/emboj/16.12.3705.

Meier, Bettina, Louise J Barber, Yan Liu, Ludmila Shtessel, Simon J Boulton, Anton Gartner, and Shawn Ahmed. 2009. “The MRT-1 Nuclease Is Required for DNA Crosslink Repair and Telomerase Activity in Vivo in Caenorhabditis Elegans.” *The EMBO Journal* 1 (22). Nature Publishing Group: 1–15. doi:10.1038/emboj.2009.278.

Morin, Gregg B. 1989. “The Human Telomere Terminal Transferase Enzyme Is a Ribonucleoprotein That Synthesizes TTAGGG Repeats.” *Cell* 59 (3): 521–29. doi:10.1016/0092-8674(89)90035-4.

Moyzis, R K, J M Buckingham, L S Cram, M Dani, L L Deaven, M D Jones, J Meyne, R L Ratliff, and J R Wu. 1988. “A Highly Conserved Repetitive DNA Sequence, (TTAGGG)n, Present at the Telomeres of Human Chromosomes.” *Proceedings of the National Academy of Sciences of the United States of America* 85 (18): 6622–26. doi:10.1073/pnas.85.18.6622.

Palm, Wilhelm, and Titia de Lange. 2008. “How Shelterin Protects Mammalian Telomeres.” *Annual Review of Genetics* 42: 301–34. doi:10.1146/annurev.genet.41.110306.130350.

Raices, Marcela, Ramiro E. Verdun, Sarah A. Compton, Candy I. Haggblom, Jack D. Griffith, Andrew Dillin, and Jan Karlseder. 2008. “C. Elegans Telomeres Contain G-Strand and C-Strand Overhangs That Are Bound by Distinct Proteins.” *Cell* 132 (5): 745–57. doi:10.1016/j.cell.2007.12.039.

Schindelin, Johannes, Ignacio Arganda-Carreras, Erwin Frise, Verena Kaynig, Mark Longair, Tobias Pietzsch, Stephan Preibisch, et al. 2012. “Fiji: An Open-Source Platform for Biological-Image Analysis.” *Nature Methods* 9 (7): 676–82. doi:10.1038/nmeth.2019.

Sfeir, Agnel, and Titia de Lange. 2012. “Removal of Shelterin Reveals the Telomere End-Protection Problem.” *Science (New York, N.Y.)* 336 (6081): 593–97. doi:10.1126/science.1218498.

Shtessel, Ludmila, Mia Rochelle Lowden, Chen Cheng, Matt Simon, Kyle Wang, and Shawn Ahmed. 2013. “Caenorhabditis Elegans POT-1 and POT-2 Repress Telomere Maintenance Pathways.” *G3 (Bethesda, Md.)* 3 (2): 305–13. doi:10.1534/g3.112.004440.

Sulston, J. E., E. Schierenberg, J. G. White, and J. N. Thomson. 1983. “The Embryonic Cell Lineage of the Nematode Caenorhabditis Elegans.” *Developmental Biology* 100 (1): 64–119. doi:10.1016/0012-1606(83)90201-4.

Takai, Kaori K., Sarah Hooper, Stephanie Blackwood, Rita Gandhi, and Titia de Lange. 2010. “In Vivo Stoichiometry of Shelterin Components.” *Journal of Biological Chemistry* 285 (2): 1457–67. doi:10.1074/jbc.M109.038026.

Thompson, Owen, Mark Edgley, Pnina Strasbourger, Stephane Flibotte, Brent Ewing, Ryan Adair, Vinci Au, et al. 2013. “The Million Mutation Project: A New Approach to Genetics in Caenorhabditis Elegans.” *Genome Research* 23 (10): 1749–62. doi:10.1101/gr.157651.113.

Timmons, L, and a Fire. 1998. “Specific Interference by Ingested dsRNA.” *Nature* 395 (6705): 854. doi:10.1038/27579.

Wicky, C, a M Villeneuve, N Lauper, L Codourey, H Tobler, and F Müller. 1996. “Telomeric Repeats (TTAGGC)n Are Sufficient for Chromosome Capping Function in Caenorhabditis Elegans.” *Proceedings of the National Academy of Sciences of the United States of America* 93 (August): 8983–88. doi:10.1073/pnas.93.17.8983.